Article

Cell Reports

Increased Polyubiquitination and Proteasomal Degradation of a Munc18-1 Disease-Linked Mutant Causes Temperature-Sensitive Defect in Exocytosis

Graphical Abstract

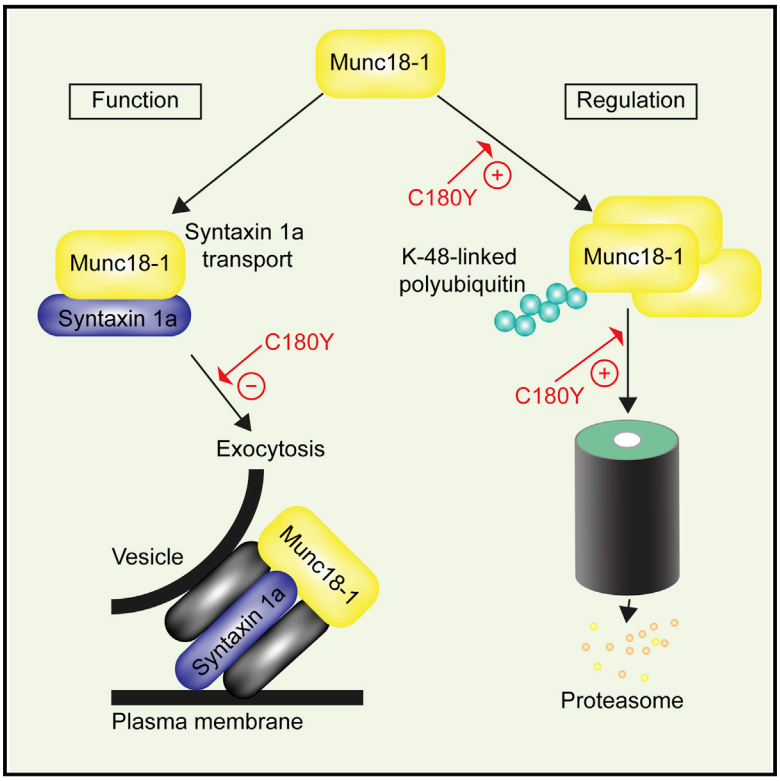

Highlights

Munc18-1C180Y mutation increases polyubiquitination and proteasome degradation

Munc18-1C180Y forms oligomers and high-molecular-weight aggregates

Munc18-1C180Y can bind syntaxin 1a but is defective in membrane fusion at 37°C

Defective membrane fusion is rescued at a lower, permissive temperature

Authors

Sally Martin, Andreas Papadopulos, ..., Brett M. Collins, Frederic A. Meunier

Correspondence

s.martin@uq.edu.au (S.M.),
f.meunier@uq.edu.au (F.A.M.)

In Brief

Mutations in Munc18-1, an essential component of the machinery controlling neurotransmission, are linked to the development of early infantile epileptic encephalopathy (EIEE). In this study, Martin et al. show that one of these mutations, C180Y, results in a thermolabile protein with a strong propensity to aggregate. The level of Munc18-1C180Y is regulated by K48-linked polyubiquitination and proteasomal degradation. The impaired exocytic function of Munc18-1C180Y is rescued by growth at a permissive temperature. An imbalance in exocytosis could therefore underpin EIEE.

Martin et al., 2014, Cell Reports 9, 206–218
October 9, 2014 ©2014 The Authors
http://dx.doi.org/10.1016/j.celrep.2014.08.059

OPEN ACCESS
CellPress

Cell Reports
Article

Increased Polyubiquitination and Proteasomal Degradation of a Munc18-1 Disease-Linked Mutant Causes Temperature-Sensitive Defect in Exocytosis

Sally Martin,[1,*] Andreas Papadopulos,[1] Vanesa M. Tomatis,[1] Emma Sierecki,[2] Nancy T. Malintan,[1] Rachel S. Gormal,[1] Nichole Giles,[2] Wayne A. Johnston,[2] Kirill Alexandrov,[2] Yann Gambin,[2] Brett M. Collins,[2] and Frederic A. Meunier[1,*]
[1]Clem Jones Centre for Ageing Dementia Research, Queensland Brain Institute, The University of Queensland, Brisbane, QLD 4072, Australia
[2]Institute for Molecular Bioscience, The University of Queensland, Brisbane, QLD 4072, Australia
*Correspondence: s.martin@uq.edu.au (S.M.), f.meunier@uq.edu.au (F.A.M.)
http://dx.doi.org/10.1016/j.celrep.2014.08.059

SUMMARY

Munc18-1 is a critical component of the core machinery controlling neuroexocytosis. Recently, mutations in Munc18-1 leading to the development of early infantile epileptic encephalopathy have been discovered. However, which degradative pathway controls Munc18-1 levels and how it impacts on neuroexocytosis in this pathology is unknown. Using neurosecretory cells deficient in Munc18, we show that a disease-linked mutation, C180Y, renders the protein unstable at 37°C. Although the mutated protein retains its function as t-SNARE chaperone, neuroexocytosis is impaired, a defect that can be rescued at a lower permissive temperature. We reveal that Munc18-1 undergoes K48-linked polyubiquitination, which is highly increased by the mutation, leading to proteasomal, but not lysosomal, degradation. Our data demonstrate that functional Munc18-1 levels are controlled through polyubiquitination and proteasomal degradation. The C180Y disease-causing mutation greatly potentiates this degradative pathway, rendering Munc18-1 unable to facilitate neuroexocytosis, a phenotype that is reversed at a permissive temperature.

INTRODUCTION

Neurotransmission is underpinned by the regulated fusion of synaptic vesicles with the plasma membrane in a process catalyzed by soluble N-ethylmaleimide-sensitive factor-attachment protein receptors (SNARE) proteins (Weber et al., 1998; Chen and Scheller, 2001). The fusion reaction is controlled by a large number of regulatory proteins (Südhof and Rizo, 2011; Jahn and Fasshauer, 2012), one of the most critical of which is the Sec1/Munc18 family protein, Munc18-1 (Toonen and Verhage, 2007; Han et al., 2010). Knockout of Munc18-1 in mice leads to perinatal paralysis-induced lethality, demonstrating the essential nature of this protein in neurotransmission (Verhage et al., 2000). Munc18-1 plays several roles in neuroexocytosis, as different conformations and complexes of the protein regulate the transport of the t-SNARE syntaxin 1a (Sx1a) to the plasma membrane, as well as the membrane fusion reaction itself (reviewed in Toonen and Verhage, 2007 and Han et al., 2010). Disruption of either of these functions prevents SNARE-mediated membrane fusion (Martin et al., 2013; Han et al., 2013). Depletion of Munc18-1 reduces the docking of secretory granules, lowers Sx1a protein levels, and leads to a mislocalization of residual Sx1a to intracellular compartments (Verhage et al., 2000; Voets et al., 2001; Arunachalam et al., 2008; McEwen and Kaplan, 2008; Han et al., 2009; Malintan et al., 2009; Papadopulos et al., 2013; Martin et al., 2013).

An additional level of regulation that could significantly impact on neuroexocytosis is the control of Munc18-1 functional expression. Although the mechanisms controlling the level of the protein are currently unknown, recent studies have suggested that mutations in Munc18-1 associated with the development of a severe early infantile epileptic encephalopathy (EIEE) (Deprez et al., 2010; Otsuka et al., 2010; Tavyev Asher and Scaglia, 2012; Barcia et al., 2014) result in a thermolabile protein with reduced expression level (Saitsu et al., 2008, 2010). As one of the characteristic features of EIEE is a pattern of "burst suppression" brain activity in electroencephalograms, where periods of intense neurological activity are interspersed with periods of profound brain inactivity, one possible contributing factor could be an imbalance in neurotransmission, due to reduced functional levels of Munc18-1.

In this study, we set out to identify the mechanisms regulating the levels of functional Munc18-1 and to analyze how a point mutation, C180Y, directly linked to the development of EIEE, affected this regulation. We show that Munc18-1 undergoes K48-linked polyubiquitination, which directs its degradation through the proteasomal system. Our results further show that temperature-sensitive structural changes associated with the C180Y mutation result in the generation of protein oligomers and aggregates and potentiate its degradation through the proteasome, leading to severely reduced functional Munc18-1 levels. Interestingly, the reduced Munc18-1 expression impairs its function in membrane fusion, although sufficient Munc18-1 activity is retained in order to mediate its Sx1a chaperone activity. Consistent with protein misfolding, a shift to a lower, permissive

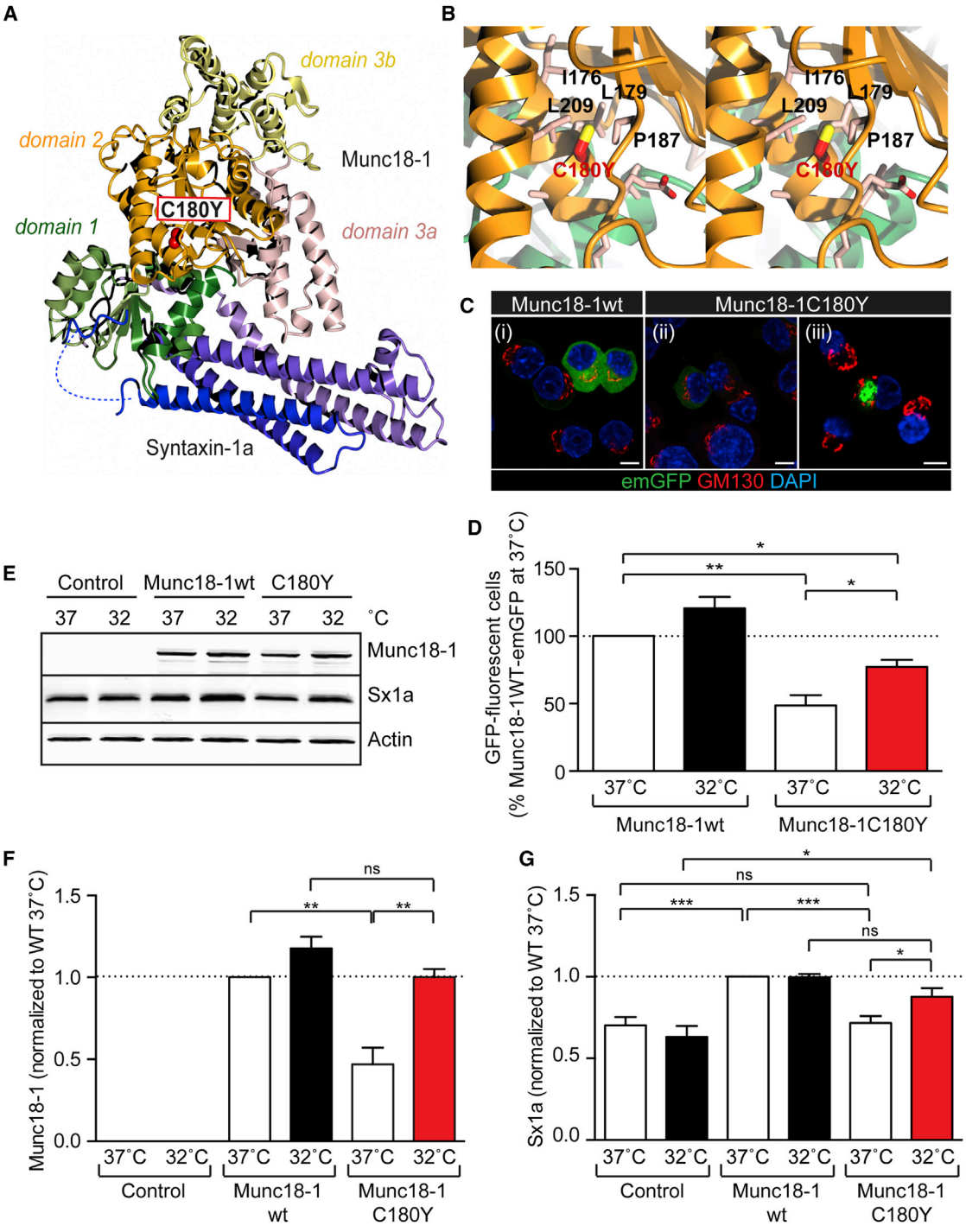

Figure 1. Munc18-1C180Y Levels Are Reduced Relative to Wild-Type but Can Be Recovered by Growth at a Permissive Temperature with the Concomitant Rescue of Sx1a

(A and B) Munc18-1 in a complex with the soluble region of closed Sx1a as solved by X-ray crystallography (Burkhardt et al., 2008). (A) The Cys180 > Tyr mutation is located within domain 2 of Munc18-1, as indicated by red spheres, with no direct interaction with Sx1a (blue). (B) Close-up stereoexamination shows that Cys180 is buried within a highly hydrophobic region of the Munc18-1 protein.

(C–G) DKD-PC12 cells were transfected with control vector, Munc18-1 wild-type (wt)-emGFP, or Munc18-1C180Y-emGFP for 48 hr, prior to incubation at 37°C or 32°C for 24 hr. (C) Cells incubated at 37°C were fixed, immunolabeled for the Golgi marker GM130, and the nuclei stained using DAPI. emGFP was imaged under identical conditions for cytosolic labeling (i and ii) or at low laser intensity for aggresomes (iii). The scale bar represents 5μm. (D) Cells were fixed and the nuclei

(legend continued on next page)

temperature fully restores the function of Munc18-1 in membrane fusion. Our results suggest that the C180Y mutation could generate large cellular aggregates, leading to an imbalance in neurotransmission in key areas of the brain at physiological temperature, by reducing the level of functional activity required to support SNARE-mediated membrane neuroexocytosis.

RESULTS

An EIEE-Linked Mutant of Munc18-1 Is Stabilized at Permissive Temperature, Supports the Transport of Sx1a to the Plasma Membrane in DKD-PC12 Cells, and Binds Normally to Sx1a In Vitro

Several mutations in Munc18-1 have been directly linked to the development of EIEE (Saitsu et al., 2008, 2010; Mignot et al., 2011). We conducted a detailed analysis of the function and regulation of one of these mutations, a Cys > Tyr point mutation (C180Y), buried in the hydrophobic core of Munc18-1 domain 2 (Figures 1A and 1B). As Munc18-1C180Y exhibits a melting temperature very close to normal physiological temperature compared to wild-type Munc18-1 (Munc18-1WT) (Saitsu et al., 2008), we considered whether Munc18-1C180Y could encode for a temperature-sensitive mutation. To examine this further, we attempted to rescue Munc18-1C180Y-emerald GFP (emGFP) expression levels in PC12 cells engineered to knock down Munc18-1 and Munc18-2 (DKD-PC12) by reducing the growth temperature to the more-permissive 32°C.

DKD-PC12 cells were transfected with Munc18-1WT-emGFP or Munc18-1C180Y-emGFP and incubated for 48 hr at 37°C. Each transfection was subsequently split and incubated at either 37°C or 32°C for a further 24 hr prior to fixation and processing for immunofluorescence microscopy (Figures 1C and 1D) or preparation of whole-cell lysates for immunoblotting (Figures 1E–1G). Consistent with previous reports (Saitsu et al., 2010), we found that, following transient transfection, Munc18-1C180Y had a significantly reduced expression level relative to the wild-type protein, which could be detected as both a decrease in total protein expression (Figure 1E) and reduced emGFP fluorescence by confocal microscopy (Figure 1C). To examine this further, we first quantified the proportion of cells showing detectable emGFP fluorescence (Figure 1D). We found that, following growth at 37°C, there were significantly fewer cells expressing detectable levels of Munc18-1C180Y-emGFP than Munc18-1WT-emGFP. Lowering the growth temperature to 32°C for 24 hr resulted in a significant increase in the number of cells with detectable Munc18-1C180Y-emGFP fluorescence. In addition, we also noted significant differences in the distribution of this fluorescence. Although both Munc18-1WT-emGFP and Munc18-1C180Y-emGFP were predominantly detected in the cytosol (Figure 1C), a subset of cells (~20%; also see Figure 5F) also contained Munc18-1C180Y-emGFP in large, fluorescent aggregates that localized to the juxtanuclear region, directly adjacent to the Golgi complex (Figure 1C). Identical phenotypes were observed when Munc18-1C180Y-emGFP was expressed in wild-type PC12 cells, or was expressed at 32°C, confirming that this phenotype was intrinsic to the mutation itself and in good agreement with the reported lower expression of Munc18-1C180Y in N2a cells (Saitsu et al., 2010).

One of the key features observed in Munc18-depleted DKD-PC12 cells is a concomitant reduction in the level of Sx1a protein (Figure S1; Verhage et al., 2000; Arunachalam et al., 2008; McEwen and Kaplan, 2008; Han et al., 2009). We therefore tested whether reducing the growth temperature could rescue the expression levels of both expressed Munc18-1 (Figure 1F) and endogenous Sx1a (Figure 1G). Consistent with previous studies, endogenous Sx1a expression was significantly rescued in DKD-PC12 cells following the re-expression of Munc18-1WT. However, no detectable rescue was observed upon Munc18-1C180Y expression. In contrast, when the cells were incubated at 32°C for 24 hr prior to analysis, there was a significant increase in the level of both Sx1a and Munc18-1C80Y-emGFP compared to growth at 37°C (Figures 1F and 1G). In fact, both Munc18-1C180Y and Sx1a were recovered at 32°C to levels indistinguishable from those obtained following expression of wild-type Munc18-1. The temperature-dependent rescue of expressed Munc18-1 and endogenous Sx1a suggests that Munc18-1C180Y retained the ability to chaperone Sx1a, a key feature requiring intact Sx1a binding.

We therefore examined the direct interaction between Munc18-1C180Y and Sx1a in vitro using purified proteins. Importantly, whereas we noted that the yield of bacterially produced recombinant Munc18-1C180Y was much lower than that of the wild-type protein, suggesting problems with protein folding and/or stability, the thermodynamic properties of Munc18-1C180Y binding to Sx1a were indistinguishable from that of wild-type as measured by isothermal titration calorimetry (Figure 2A; Table 1). Similarly, a proximity-based assay (ALPHAScreen) analysis using in vitro translated proteins (Sierecki et al., 2013, 2014; Gambin et al., 2014) could detect no difference in Sx1a binding between Munc18-1WT or Munc18-1C180Y proteins (Figures 2B–2D). Together, these data confirm that Munc18-1C180Y is able to form a binary complex with Sx1a in vitro, as suggested previously (Saitsu et al., 2008).

As the binary interaction between Munc18-1 and Sx1a is required to mediate the transport of Sx1a to the cell surface, we analyzed whether the chaperone function of Munc18-1 was affected by the mutation and temperature in DKD-PC12 cells. In control empty-vector-transfected or untransfected DKD-PC12 cells, a low level of endogenous Sx1a labeling was detected in intracellular compartments (Figures 2E–2G). In contrast, following re-expression of either Munc18-1WT-emGFP or Munc18-1C180Y-emGFP, Sx1a was predominantly present at the cell surface. Quantification of Sx1a labeling at the cell surface revealed that Munc18-1WT-emGFP and Munc18-1C180Y-emGFP were both capable of rescuing Sx1a

stained using DAPI. The number of cells containing detectable emGFP fluorescence was quantified under identical imaging conditions. *$p < 0.05$; **$p < 0.01$; results show mean ± SEM (n = 3). (E–G) Transfected cells were analyzed by western blotting and the amount of Munc18-1wt-emGFP, Munc18-1C180Y-emGFP, and Sx1a was quantified relative to β-actin. *$p < 0.05$; **$p < 0.01$; ***$p < 0.001$; results show mean ± SEM (n = 3).
See also Figure S1.

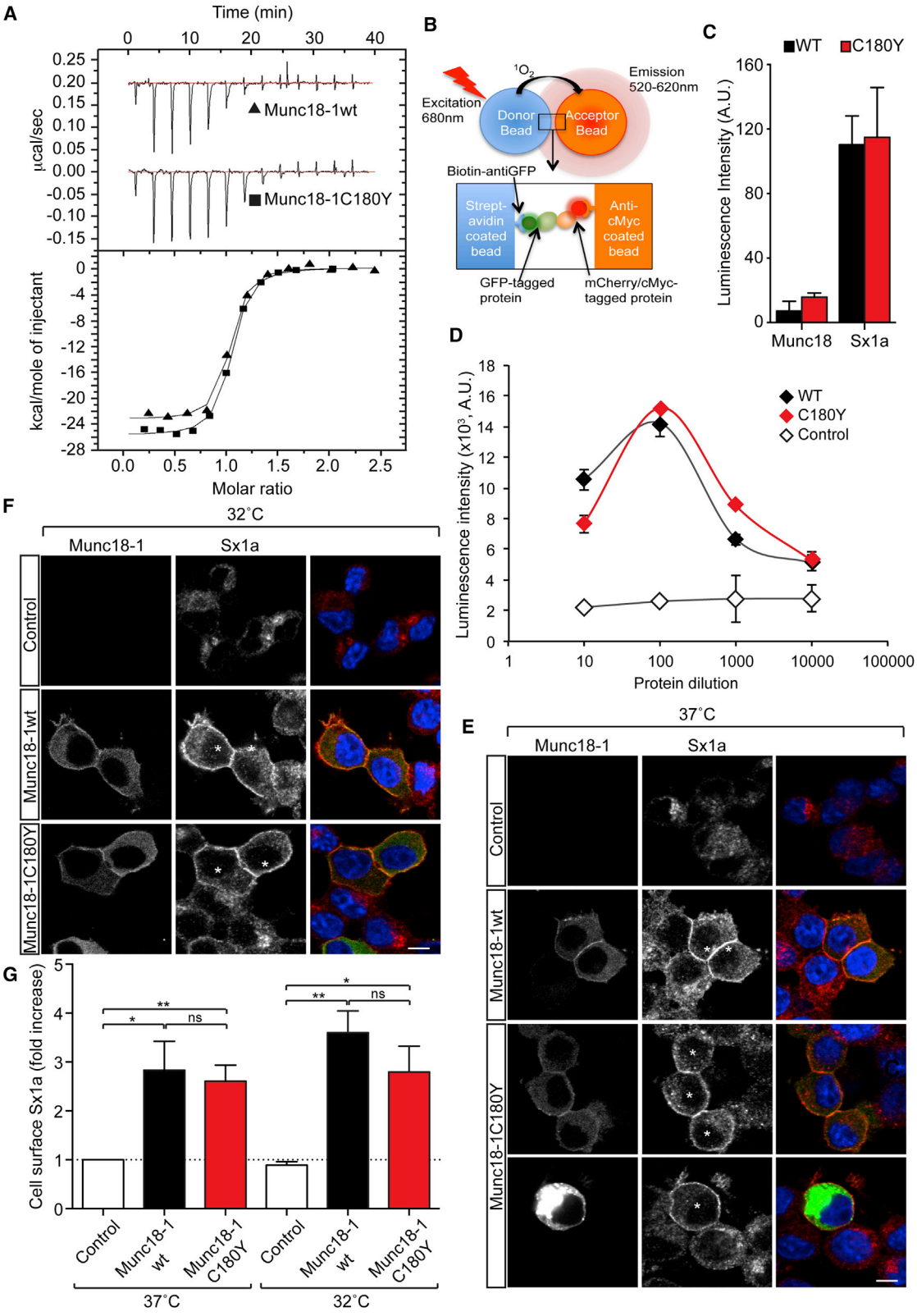

(legend on next page)

Table 1. Thermodynamic Parameters for the Binding of $Sx1a_{2-243}$ to Munc18-1WT Determined by Isothermal Titration Calorimetry

Protein Interaction	ΔH (kCal mol^{-1})	$T\Delta S$ (kCal mol^{-1})	ΔG (kCal mol^{-1})	*K*d (nM)	n
Munc18-1WT: $Sx1a_{2-243}$	−22.5 ± 0.67	−11.9 ± 0.66	−10.5 ± 0.34	19.1 ± 1.14	0.91 ± 0.03
Munc18-1C180Y: $Sx1a_{2-243}$	−23.7 ± 0.89	−13.1 ± 0.95	−10.6 ± 0.66	18.6 ± 1.71	1.02 ± 0.01

Values are expressed as mean ± SEM (n = 5). All experiments were performed at 298 K.

plasma membrane localization to the same degree (Figure 2G). Importantly, Sx1 transport was not affected by growth at different temperatures. The presence of Munc18-1C180Y-emGFP aggregates did not preclude the transport of Sx1a to the cell surface. These data confirm that Munc18-1C180Y is capable of binding to Sx1a in a binary complex and can rescue its transport to the cell surface in DKD-PC12 cells.

Munc18-1C180Y Is Unable to Rescue Stimulated Exocytosis at 37°C but Regains Full Functionality at 32°C

Our findings demonstrate that Munc18-1C180Y is capable of binding to Sx1a and transporting it to the cell surface. However, as previous studies had shown that Munc18-1C180Y has reduced binding to a mutant of Sx1a mimicking an "open" conformation primed for SNARE complex interactions (Saitsu et al., 2008), we directly analyzed its ability to rescue neuroexocytosis in DKD-PC12 cells. emGFP-tagged Munc18-1WT or Munc18-1C180Y was re-expressed in DKD-PC12 cells together with NPY-mCherry. The fusion of individual secretory granules containing NPY-mCherry with the cell surface was analyzed by total internal reflectance fluorescence (TIRF) microscopy, before and during stimulation (Figures 3A–3C). Whereas no fusion of secretory granules was detected in unstimulated cells under any condition, we found that Munc18-1WT expression restored stimulated secretory granule fusion in DKD-PC12 cells as previously described (Martin et al., 2013), regardless of growth temperature (Figures 3A–3D). In contrast, Munc18-1C180Y did not rescue secretory granule fusion at 37°C, but full restoration of neuroexocytosis was achieved when cells were incubated at 32°C for 24–48 hr prior to analysis (Figure 3D). The inability of Munc18-1C180Y to restore stimulated secretory granule fusion at 37°C did not result from a defect in secretory granule biogenesis, as there was no significant difference in the number of secretory granules between conditions, detected by measuring NPY-mCherry-containing secretory granules or following labeling for the secretory granule marker protein, synaptotagmin-1 (Figures 3E–3G). As these data suggest that the function of Munc18-1C180Y could be restored at permissive temperature, we further analyzed the ability of this mutant to rescue stimulated secretion using a biochemical assay. Munc18-1WT-emGFP or Munc18-1C180Y-emGFP was re-expressed in DKD-PC12 cells together with NPY-human placental alkaline phosphatase (hPLAP) (Martin et al., 2013; Tomatis et al., 2013; Figures 3E–3G). When the cells were incubated at 32°C for 24 hr prior to assaying, both Munc18-1WT-emGFP and Munc18-1C180Y-emGFP were able to rescue stimulated NPY release to the same extent (Figure 3H). However, following re-expression of Munc18-1C180Y at 37°C, the release of NPY-hPLAP was significantly reduced (Figure 3H). Together, these data confirm that the C180Y mutation is responsible for the temperature-dependent defect in stimulated secretion.

Munc18-1C180Y Forms Temperature-Dependent, Detergent-Insoluble Cytosolic Protein Aggregates in PC12 Cells and In Vitro

The data described above suggest that Munc18-1C180Y is a thermolabile protein that can function normally if its effective levels are increased by reducing growth temperature. We therefore further examined causes leading to the two observed phenotypes of Munc18-1C180Y: reduced cytosolic expression levels and increased aggregation.

To examine the nature of the fluorescent Munc18-1C180Y-emGFP aggregates in more detail, we used correlative light and electron microscopy. PC12 cells were transfected with either Munc18-1WT-emGFP or Munc18-1C180Y-emGFP, and fluorescent cells were identified and analyzed by transmission electron microscopy. In Munc18-1C180Y-emGFP-expressing cells,

Figure 2. Munc18-1C180Y Binds to Sx1a and Supports Its Transport to the Cell Surface

(A) Isothermal titration calorimetry of Munc18-1wt (triangles) and Munc18-1C180Y (squares) binding to Sx1a (2–243). These Sx1a residues constitute the Sx1a soluble region lacking the C-terminal transmembrane helix, which predominantly exists in a closed conformation.

(B) Schematic representation of the ALPHAScreen proximity assay. The streptavidin-coated donor bead binds biotin-coupled GFP-nanotrap that recruits GFP-tagged proteins. The acceptor bead coated with anti-myc binds to myc-tagged proteins. The donor bead releases singlet oxygen ($^1O_2$) upon illumination at 680 nm, which has a half-life of 4 μs and can diffuse ~200 nm in solution. If an acceptor bead is within that distance, $^1O_2$ reacts with derivatives in the acceptor bead and luminescence is observed at 520–620 nm. Protein:protein interactions result in a close proximity, leading to the ALPHAScreen signal.

(C) ALPHAScreen assay binding of Munc18-1WT and Munc18-1C180Y to Sx1a. Results equal average binding index ± SEM (n ≥ 3 experiments). A.U., arbitrary units.

(D) Typical ALPHAScreen data obtained for a LTE-expressed noninteracting protein pair (control, GFP-Munc18-1WT and Munc18-1WT-Cherry-myc) and for two test pairs (GFP-Sx1a:Munc18-1WT-Cherry-myc [WT] or GFP-Sx1a:Munc18-1-C180Y-Cherry-myc [C180Y]) over a range of dilutions. Results show mean ± SEM (n = 5).

(E and F) DKD-PC12 cells were transfected with control vector, Munc18-1wt-emGFP, or Munc18-1C180Y-emGFP for 48 hr, prior to incubation at 37°C or 32°C for 24 hr. Cells were fixed and labeled for Sx1a. Asterisks indicate transfected cells. The scale bar represents 5 μm.

(G) Labeling of Sx1a at the plasma membrane, shown in (E) and (F), was quantified and the level relative to control vector-transfected cells at 37°C determined. *$p < 0.05$; **$p < 0.01$; results show mean ± SEM (n = 3).

See also Figure S2.

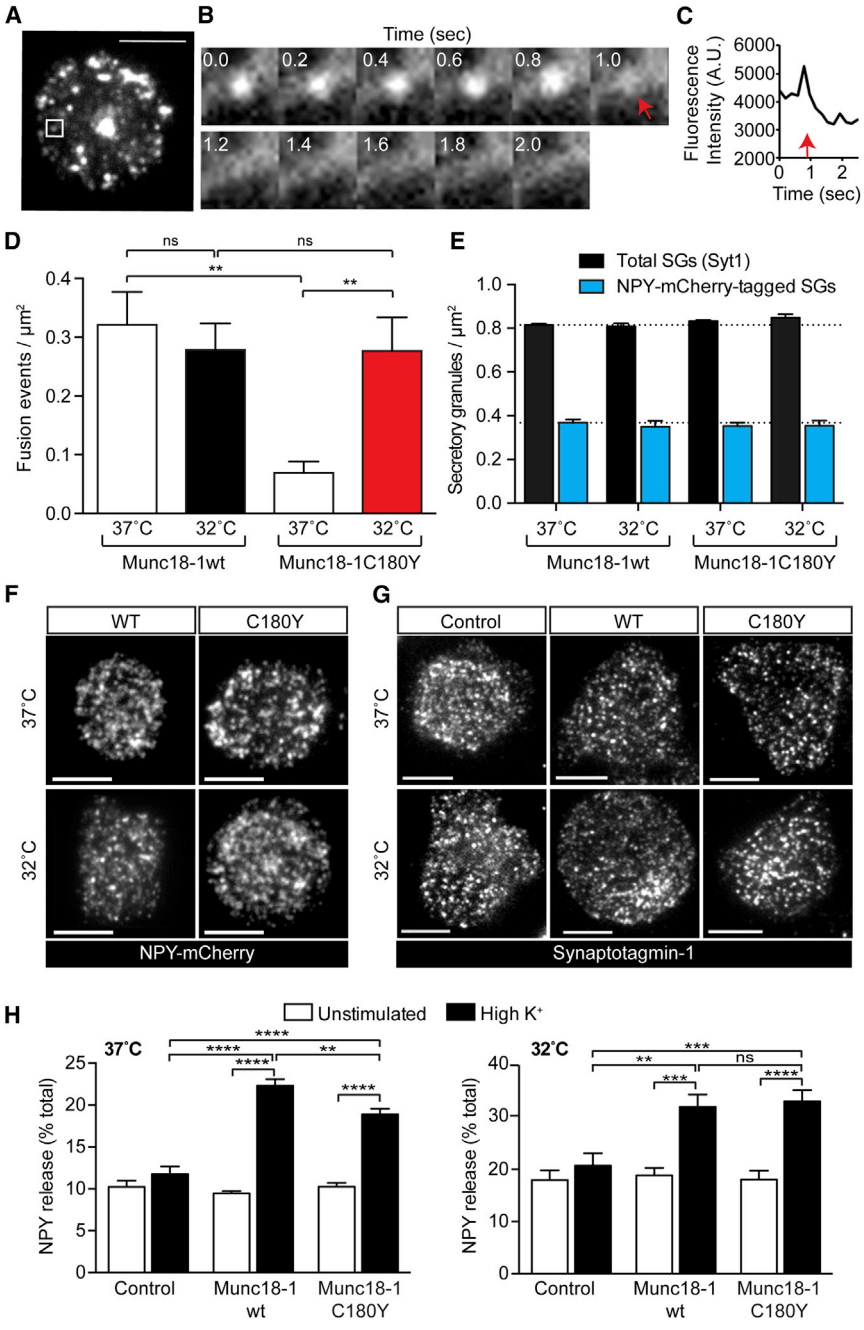

Figure 3. Munc18-1C180Y Fails to Support Full Stimulated Membrane Fusion at 37°C, a Phenotype that Can Be Rescued by Growth at 32°C

(A–D) DKD-PC12 cells were cotransfected with emGFP-tagged Munc18-1wt or Munc18-1C180Y and NPY-mCherry for 48 hr, prior to incubation at 37°C or 32°C for 24–48 hr. (A) NPY-mCherry-labeled secretory granules in the TIRF plane of a DKD-PC12 cell coexpressing Munc18-1wt-emGFP and incubated at 37°C. Enlargements (B) show a sequential 0.2 s time series containing a fusion event (red arrow) following 2 mM Ba^{2+} stimulation. The graph (C) shows the spike in fluorescence intensity observed as the secretory granule approaches the plasma membrane during the fusion event. The scale bar represents 5 µm. (D) Secretory granule fusion was imaged at 10 Hz by TIRF microscopy for 5 min following 2 mM Ba^{2+} stimulation at either 37°C or 32°C as indicated and individual fusion events quantified relative to the surface area. **$p < 0.01$; results show mean ± SEM (n = 5 independent experiments; 2 to 3 cells/experiment).

(E–G) DKD-PC12 cells were transfected with empty vector (control), Munc18-1wt-emGFP, or Munc18-1C180Y-emGFP with or without NPY-mCherry, fixed, and processed for TIRF microscopy. Cells expressing Munc18-1 constructs alone were immunolabeled for synaptotagmin-1 (Syt1). (E) The number of secretory granules (SGs) labeled with either Syt1 (total SGs) or NPY-mCherry within the TIRF plane of unstimulated cells was quantified; results show mean ± SEM (n = 5 independent experiments for NPY-mCherry; n = 3 independent experiments; 5–10 cells/experiment for Syt1). Representative TIRF images of NPY-mCherry-labeled secretory granules (F) or Syt1-labeled secretory granules (G) in unstimulated DKD-PC12 cells. The scale bar represents 5 µm.

(H) DKD-PC12 cells were cotransfected with emGFP-tagged Munc18-1, Munc18-1C180Y, or empty vector and NPY-hPLAP and incubated at 37°C or 32°C for 24 hr prior to measuring K^+-stimulated secretion over 15 min. Results show mean ± SEM. n = 3. **$p < 0.01$; ***$p < 0.001$; ****$p < 0.0001$. ns, not significant.

fluorescence was clearly correlated with the presence of extensive, electron-dense protein aggregates in the cytoplasm of the cells and clustering toward the cell nucleus (Figure 4A). The protein aggregates were not membrane bound and showed no preferential association with other organelles, including secretory granules. Consistent with the immunofluorescence microscopy shown in Figure 3, there was also no effect of Munc18-1C180Y expression on the number or docking of secretory granules in cells containing large protein aggregates (Figure 4B and 4C). The extent of the aggregate accumulation varied between cells, with some cells showing a high abundance of aggregates whereas other cells had low or undetectable aggregation. No protein aggregates were detected in control, untransfected cells, or in cells expressing Munc18-1WT-emGFP.

To determine the biochemical nature of the Munc18-1C180Y aggregates, we analyzed their solubility in denaturing (SDS) and nondenaturing (Triton X-100) detergents. We found that Munc18-1C180Y was highly resistant to solubilization in 1% Triton X-100, with less than 10% recovered relative to the whole-cell lysate (Figures 4D and 4E). This low percentage of recoverable Munc18-1C180Y was surprising, as confocal microscopy had shown that only a small percentage of the Munc18-1C180Y-transfected cells contained detectable fluorescent aggregates. This suggests that Munc18-1C180Y may also be present in much-smaller, detergent-insoluble

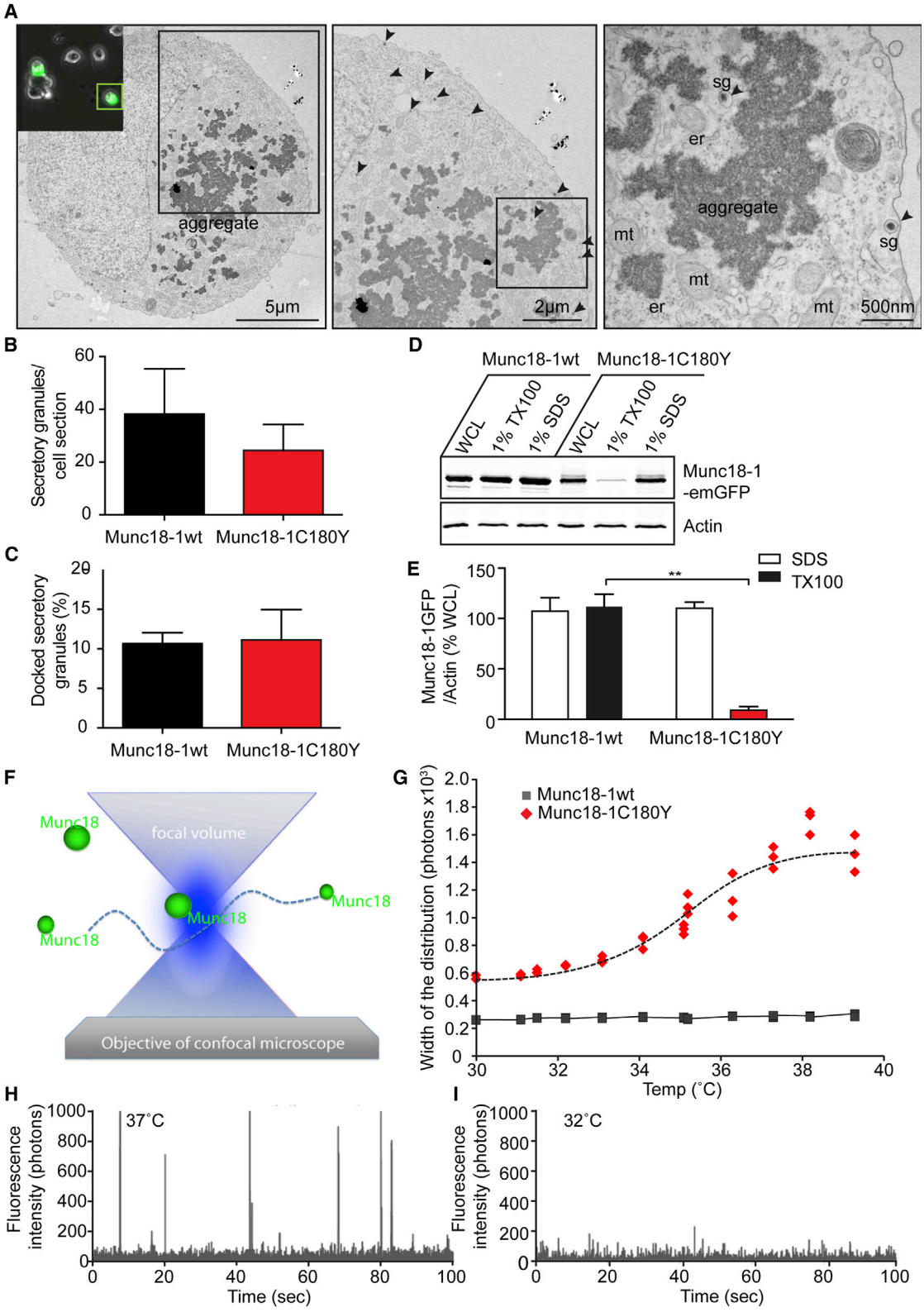

(legend on next page)

oligomers in the cytosol, below the resolution limit of light microscopy.

To examine the process leading to Munc18-1C180Y aggregation, we used single-molecule fluorescence spectroscopy to directly assess protein oligomerization of in vitro synthesized proteins (Figures 4F–4I; Gambin et al., 2014). Fluorescently tagged Munc18-1WT and Munc18-1C180Y were expressed in a eukaryotic-cell-free system (Figure S2A), and the fluorescence intensity of single, freely diffusing molecules in a defined confocal volume was measured (Figure 4F). To determine the effect of temperature, cell-free extracts were incubated between 30°C and 40°C for 30 min prior to imaging and time traces analyzed for the presence of aggregates by determining the distribution of values around the average fluorescence (Figures 4G and S2B). In the case of folded monomeric Munc18-1, the variations in the intensity as monomers entered and left the focal volume were small. When aggregates were present, the bright particles created large fluctuations of intensity (Figure 4H). By calculating the distribution of intensity values and measuring their SD, we were able to measure protein aggregation. As shown in Figure 4G, this parameter remained low for Munc18-1WT but increased significantly with increasing temperature for Munc18-1C180Y. Individual time traces for Munc18-1C180Y incubated at either 32°C or 37°C clearly showed the increasing propensity to form aggregates at 37°C (Figure 4H).

Munc18-1C180Y Is K48 Polyubiquitinated and Degraded by the Proteasome, and Aggregated Protein Rapidly Accumulates near the Microtubule-Organizing Center following Proteasome Inhibition

Protein aggregation is often considered a protective response to the presence of misfolded proteins in the cytosol. Although protein aggregates themselves are often degraded by the lysosomal system through incorporation into autophagosomes (Knaevelsrud and Simonsen, 2010; Yamamoto and Simonsen, 2011), another efficient mechanism to dispose of misfolded proteins is the 26S proteasome (Wickner et al., 1999). To determine the mechanism underpinning Munc18-1C180Y degradation, PC12 cells were transfected with either Munc18-1WT-emGFP or Munc18-1C180Y-emGFP and incubated with proteasome (MG132) or lysosome (NH_4Cl or bafilomycin A_1) inhibitors (Figures 5A–5C). Consistent with the majority of Munc18-1C180Y being degraded by the proteasome, we observed a significant increase in the level of Munc18-1C180Y in the presence of the proteasomal, but not the lysosomal, inhibitors. No significant increase in the level of Munc18-1WT-emGFP was observed.

To examine the effect of proteasome inhibition on the distribution of mutated Munc18-1, PC12 cells were transfected with Munc18-1WT-emGFP or Munc18-1C180Y-emGFP and treated with or without 2.5 μM MG132 up to 4 hr prior to fixation for immunofluorescence microscopy. Although this treatment had no effect on the distribution of Munc18-1WT-emGFP, there was a significant redistribution of Munc18-1C180Y-emGFP from a diffuse, predominantly cytosolic distribution, to an intense concentration in the dispersed microaggregates and/or into two bright aggregates at the perinuclear region of the cell (Figures 5D and 5E). Interestingly, the appearance of the perinuclear aggregates preceded the appearance of dispersed microaggregates by several hours, suggesting the presence of preexisting aggregated material. The proportion of cells containing either large perinuclear aggresomes or large dispersed aggregates was unchanged (Figure 5F). Colabeling with γ-tubulin, a marker of the microtubule-organizing center, confirmed that Munc18-1C180Y was predominantly accumulating in this region of the cell (Figure 5G). This distribution is consistent with Munc18-1C180Y in the periphery being associated with small aggresomes, which undergo microtubule-based translocation toward the proteasome (Wiese and Zheng, 2006).

Degradation of proteins by the proteasome is encoded by polyubiquitination following the attachment of K48-linked polyubiquitin chains (Komander and Rape, 2012). We therefore investigated the ubiquitination status of Munc18-1WT-emGFP and Munc18-1C180Y-emGFP, both in control cells and following inhibition of the proteasome for up to 24 hr (Figures 6A and 6B). Consistent with previous data (Figure 5A), Munc18-1C180Y showed a significant increase in expression after inhibition of the proteasome for 8 hr that was further increased after 24 hr (Figures 6A and 6B). Concomitantly, there was a decrease in the proportion of Triton-X-100-soluble Munc18-1C180Y and an

Figure 4. Munc18-1C180Y Is Detergent Insoluble and Forms Cytosolic Aggregates

(A) PC12 cells were transfected with Munc18-1C180Y-emGFP, fixed, and processed for correlative light and electron microscopy. Cells with high-Munc18-1C180Y-emGFP fluorescence were found to contain varying amounts of electron-dense, cytosolic protein aggregates that were not observed in control cells. er, endoplasmic reticulum; mt, mitochondria; sg, secretory granules (also marked with arrowheads).

(B and C) The high levels of aggregated protein in the Munc18-1C180Y-emGFP transfected cells did not affect either the number or docking of secretory granules relative to Munc18-1wt-emGFP-expressing cells; results show mean ± SEM (n = 15–20 cells per condition).

(D) PC12 cells were transfected with Munc18-1wt-emGFP or Munc18-1C180Y-emGFP. Whole-cell lysates (WCL) were extracted with 1% Triton X-100 (TX100) or 1% SDS, and samples were analyzed by SDS-PAGE and western blotting for Munc18-1 and β-actin.

(E) The level of protein expression shown in (D) was quantified relative to β-actin and normalized to the whole-cell lysate samples. $^{**}p < 0.01$; results show mean ± SEM (n = 3).

(F) Munc18-1 brightness analysis principle: GFP-tagged, LTE-expressed Munc18-1wt or Munc18-1C180Y was diluted to nM concentration and allowed to diffuse freely in solution. Fluorescent proteins were detected upon entry in the confocal volume created by a 488 nm laser focused by a 40×/1.2 numerical aperture microscope objective.

(G) Aggregation of Munc18-1wt and Munc18-1C180Y as a function of temperature. Munc18-1wt (gray squares) and Munc18-1C180Y (red diamonds) were expressed in LTE for 2 hr before being incubated at between 30°C and 40°C for 15 min. Samples were then diluted and subjected to brightness analysis. The width of the photon distribution was used as a measure of aggregation propensity with increasing temperature.

(H and I) Representative fluorescence time traces for single, freely diffusing Munc18-1C180Y molecules. The fluorescence intensity (photons/ms) is plotted as a function of time. (H) Aggregates were clearly detected in Munc18-1C180Y-GFP samples incubated at 37°C for 30 min.

See also Figure S3.

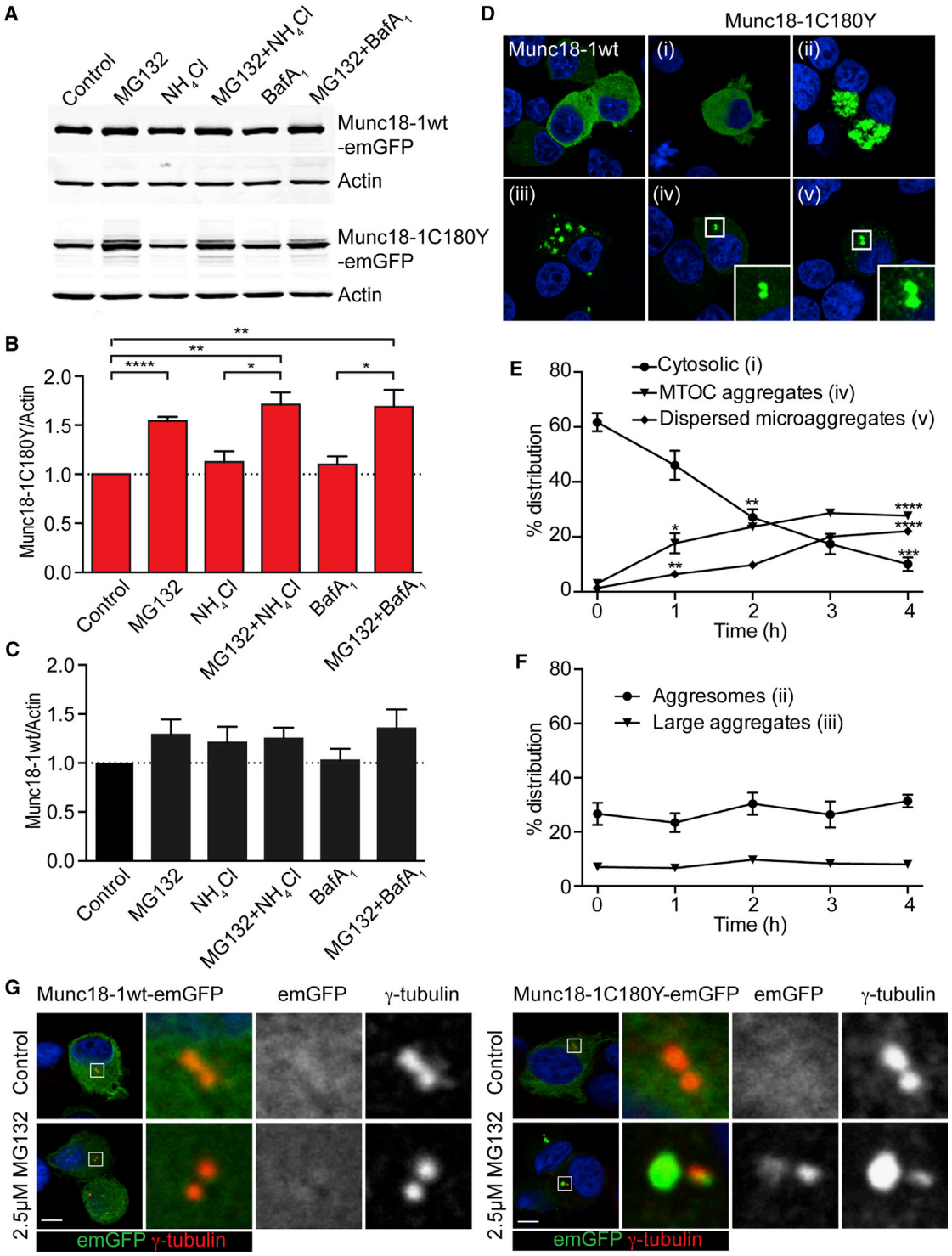

Figure 5. Proteasome Inhibition Leads to Munc18-1C180Y Aggregation at the Microtubule-Organizing Center

(A) PC12 cells transfected with Munc18-1wt-emGFP or Munc18-1C180Y-emGFP were cultured for 24 hr before being treated singly or in combination with 2.5 μM MG132, 25 mM NH_4Cl, 200 nM Bafilomycin A_1 (Baf A_1), or vehicle (control) for 24 hr. Samples were analyzed by western blotting for Munc18-1 and β-actin.

(B and C) The level of protein expression as shown in (A) was analyzed relative to β-actin and normalized to control untreated samples. *$p < 0.05$; **$p < 0.001$; results show mean ± SEM (n = 3).

(D–F) PC12 cells transfected with Munc18-1wt-emGFP or Munc18-1C180Y-emGFP were cultured for 48 hr prior to addition of 2.5 μM MG132 or an equivalent volume of DMSO (control) for various times up to 4 hr. Cells were fixed and stained for DAPI. The scale bar represents 5 μm. (D) Five distinct distributions of

(legend continued on next page)

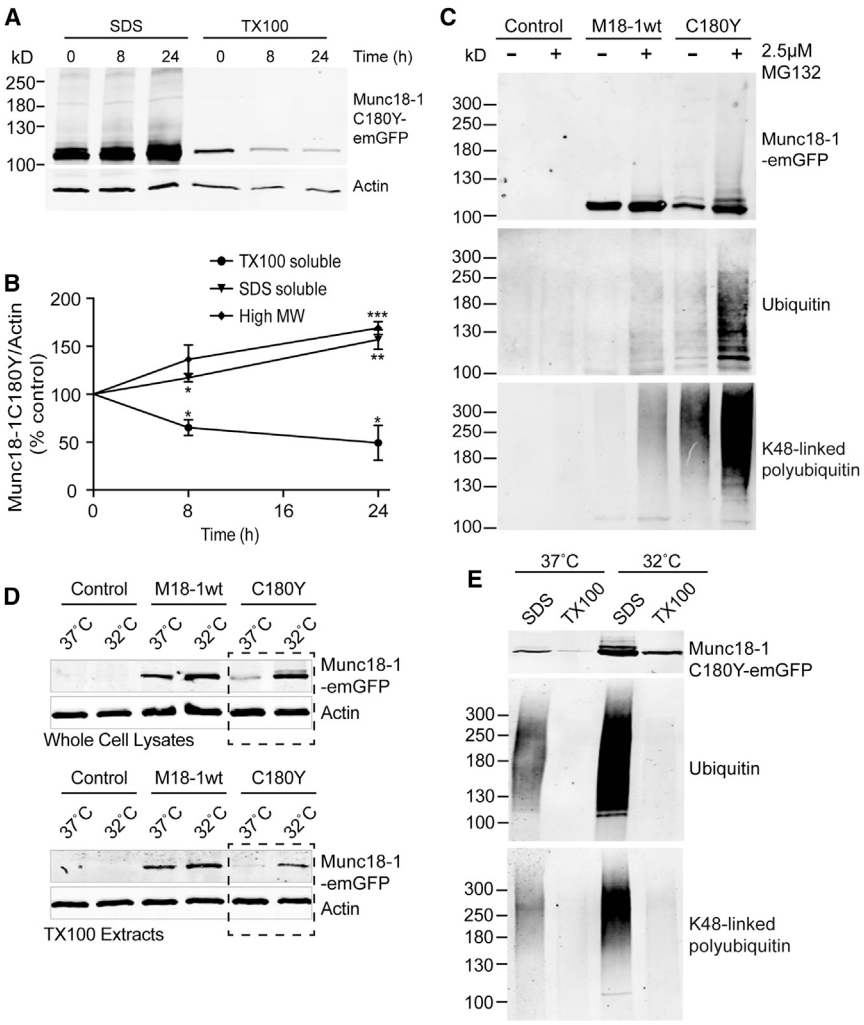

Figure 6. Ubiquitination of Aggregated Munc18-1C180Y

(A–C) PC12 cells were transfected with control vector, Munc18-1wt-emGFP, or Munc18-1C180Y-emGFP and cultured for 48 hr prior to addition of 2.5 μM MG132 or an equivalent volume of DMSO for 8 hr or 24 hr. (A) Cells were extracted with 1% Triton X-100 (TX100) or 1% SDS and analyzed by SDS-PAGE and western blotting for Munc18-1 and β-actin. (B) The level of protein expression shown in (A) was quantified relative to β-actin and normalized to starting levels (time 0). High-molecular-weight (MW) Munc18-1 was quantified from the fluorescent signal between 130 and 250 kD. *$p < 0.05$; **$p < 0.01$; ***$p < 0.001$; results show mean ± SEM (n = 3) relative to time 0. (C) Immunoprecipitation using GFP-nanotrap demonstrated increased K48-linked polyubiquitination of Munc18-1C180Y-emGFP under control conditions, which was highly augmented by inhibition of the proteasome.

(D and E) PC12 cells were transfected with control vector, Munc18-1wt-emGFP, or Munc18-1C180Y-emGFP for 24 hr prior to incubation at 37°C or 32°C for 72 hr. (D) Whole-cell lysates were extracted with 1% Triton X-100 (TX100) or 1% SDS, and samples were analyzed by SDS-PAGE and western blotting for Munc18-1 and β-actin. (E) Munc18-1C180Y-emGFP was also immunoprecipitated from SDS or Triton X-100 extracts of whole-cell lysates (highlighted fractions in D) using GFP-nanotrap and immunoblotted for Munc18-1, ubiquitin, and K-48-linked polyubiquitin.

increase in the presence of high-molecular-weight Munc18-1C180Y species (Figures 6A and 6B). No change in the expression of Munc18-1WT was observed (Figure S3). The presence of high-molecular-weight Munc18-1C180Y upon proteasome inhibition was strongly suggestive of polyubiquitination. The lysates were therefore subsequently analyzed for polyubiquitination following solubilization in SDS to extract the aggregates prior to immunoprecipitation using GFP-trap (Martin et al., 2013). As predicted, and despite its low expression, we found that Munc18-1C180Y was highly polyubiquitinated and highly labeled for K48-linked polyubiquitin (Figure 6C). In contrast, Munc18-1WT-emGFP showed no significant polyubiquitination in control conditions (Figure 6C). Following inhibition of the proteasome, there was a significant increase in the ubiquitination of both Munc18-1WT and Munc18-1C180Y. Together, these data confirm that Munc18-1C180Y is not only unstable and prone to misfolding but also degraded by the proteasome system following K48-linked polyubiquitination. Furthermore, the small increase in polyubiquitinated Munc18-1WT following proteasome inhibition suggests that degradation by the proteasome is a physiological component of the regulation of Munc18-1 expression.

To investigate the relationship between polyubiquitination and functional Munc18-1C180Y expression, we examined the distribution of polyubiquitinated protein between the soluble and the insoluble pools. Consistent with our previous data (Figure 1), we were able to increase the amount of soluble Munc18-1C180Y-emGFP by maintaining the cells at 32°C for 72 hr (Figure 6D). We subsequently immunoprecipitated Munc18-1C180Y from the SDS-soluble and Triton-X-100-soluble fractions and analyzed its ubiquitination. Interestingly, we found that the soluble pool of Munc18-1C180Y showed significantly reduced polyubiquitination relative to the insoluble pool at

Munc18-1C180Y-emGFP were observed following proteasome inhibition (i–v). There was no change in the distribution of Munc18-1wt-emGFP. (E and F) The relative proportion of cells with each distribution of Munc18-1C180Y-emGFP was quantified. *$p < 0.05$; **$p < 0.01$; ***$p < 0.001$; ****$p < 0.0001$; results show mean ± SEM (n = 3 independent experiments; ~150–500 cells/expt).

(G) PC12 cells transfected with Munc18-1wt-emGFP or Munc18-1C180Y-emGFP were cultured for 48 hr prior to the addition of 2.5 μM MG132 or an equivalent volume of DMSO (control) for 4 hr. Cells were fixed and labeled for γ-tubulin. The scale bar represents 5 μm.

permissive temperature (Figure 6E). These data show that the C180Y mutation greatly accelerates polyubiquitination and proteasomal degradation, leading to reduced Munc18-1 levels. Our results also indicate that polyubiquitination is an important factor regulating the expression level of Munc18-1WT.

DISCUSSION

In the current study, we provided a detailed analysis of the effect of an EIEE-linked Munc18-1 point mutation (C180Y) on the dual function and cellular regulation of Munc18-1. Previous studies have suggested that this mutation can directly affect binding to Sx1a and that the protein has a propensity to form aggregates, consistent with misfolding (Saitsu et al., 2008). We found that Munc18-1C180Y is able to bind Sx1a with an equal efficiency to the wild-type protein, restoring normal levels of Sx1a at the plasma membrane. However, the correct folding of Munc18-1C180Y in vitro is highly temperature-sensitive, resulting in elevated levels of aggregation at temperatures above 32°C. In neurosecretory cells, Munc18-1C180Y is similarly unstable, forming detergent-insoluble, cytosolic protein aggregates. The removal of misfolded Munc18-1C180Y in cells is regulated by K48-linked polyubiquitination and proteasomal degradation. The disease-associated variant is unable to facilitate stimulated exocytosis or to stabilize Sx1a expression, suggesting the function of Munc18-1C180Y in membrane fusion is impaired. Consistent with a temperature-sensitive misfolding of Munc18-1C180Y, growth at lower, permissive temperature fully restores its function in terms of both Sx1a expression and membrane fusion.

Our data suggest that the C180Y mutation can induce a structural change in the protein that destabilizes normal protein folding, potentiating its degradation through the proteasome. This is completely consistent with the location of the Cys180 side chain, which is tightly buried within the hydrophobic core of domain 2 (Figures 1A and 1B). Introduction of a bulky Tyr side chain in this site will significantly perturb normal hydrophobic packing within this domain. Although this mutation can perturb protein folding, leading to protein aggregation, it is not entirely clear why the Sx1a chaperone function remains normal in cells expressing Munc18-1C180Y, whereas membrane fusion and exocytosis are inhibited. Previous studies suggest that the C180Y mutation can specifically interfere with the binding of Sx1a in the open state, primed for SNARE complex formation, but not in the closed state required for Sx1a trafficking (Saitsu et al., 2008). Our data are consistent with this model, although it is difficult to understand how this could occur mechanistically, as the C180Y mutation in domain 2 is located distally from any known Sx1a-binding sites (Figure 1A). An alternative explanation for our data is that the mutation leads to lowered total levels of functional Munc18-1 in the cell and that a greater level of Munc18-1 is required to promote membrane fusion than is necessary for stabilizing Sx1a levels at the cell surface. Further work will be required to discriminate between these possibilities.

Mean core body temperature is tightly regulated and ranges between 36.5°C and 37.5°C. Circular dichroism measurements of purified, recombinant Munc18-1C180Y demonstrated that the stability of the secondary structure was slightly reduced relative to the Munc18-1WT protein and further showed that the thermostability was lower, with a protein melting temperature of ~38.5°C (Saitsu et al., 2008). Consistent with temperature-sensitive misfolding, we have shown that the inability of Munc18-1C180Y to facilitate membrane fusion manifest at 37°C can be rescued by incubation at 32°C. The existence of temperature-sensitive mutations underlying the development of different types of neurological disorders, including epilepsy and febrile seizures, is not restricted to Munc18-1. Various mutations in the voltage-gated sodium channel, *SCN1A* ($Na_v1.1$), associated with EIEE type 6, also known as Dravet syndrome or severe myoclonic epilepsy of infancy, as well as with the more benign pediatric epilepsy, generalized epilepsy with febrile seizures plus (reviewed in Escayg and Goldin, 2010 and Egri and Ruben, 2012), can also have a temperature-sensitive phenotype. Our data provide a clear demonstration that a human disease mutation in Munc18-1WT produces a defect in neuroexocytosis that can be rescued at a lower, permissive temperature.

A number of Munc18-1 EIEE-linked mutations, including C180Y, have been shown to have a tendency to form aggregates in N2a cells (Saitsu et al., 2008) and PC12 cells (this study). However, the lack of association between protein aggregates and neuronal cell death has led to the hypothesis that aggresome formation could be a protective mechanism and that most toxicity is encoded within smaller oligomeric intermediates (Price and Morris, 1999; Berke and Paulson, 2003). Despite the low apparent abundance of Munc18-1C180Y aggregates in PC12 cells, we found that the majority of the protein was insoluble, consistent with the formation of smaller, morphologically undetectable, detergent-insoluble oligomers.

Polyubiquitination can target proteins to different endpoints, depending upon the biochemical nature of the ubiquitin chains (Komander and Rape, 2012). K48-linked polyubiquitin is predominantly involved in targeting proteins for degradation by the proteasome. Our demonstration that Munc18-1WT and Munc18-1C180Y both label with K48-linked polyubiquitin is clearly suggestive of a role for proteasomal degradation in the normal regulation of Munc18-1 levels. This is in good agreement with the recent finding (from a proteomics screen) that Munc18-1 is ubiquitinated (Pridgeon et al., 2009). Further work will be needed to identify the Munc18-1 ubiquitinated residue(s) and the functional consequences of such ubiquitination. Interestingly, the presence of distinct lower-molecular-weight (MW) ubiquitinated bands in the Munc18-1WT and Munc18-1C180Y immunoprecipitations suggests that Munc18-1 could also undergo monoubiquitination (Figures 6C and 6E). Further studies will be needed to determine whether this is indeed the case and, if so, to address the functional relevance of such modifications.

Together, our data demonstrate that Munc18-1-C180Y protein instability leads to a potentiation of Munc18-1 proteasomal degradation and altered neuroexocytosis. Future studies will be needed to demonstrate that such an alteration is directly or indirectly linked to the generation of bursts suppressions due to imbalanced neurotransmission in key areas of the brain. The temperature sensitivity of the mutation also suggests that therapies designed to temporarily alter the temperature of the brain could potentially affect functional levels of Munc18-1C180Y. The data in the current study are beginning to shed light on

some of the pathological features underlying the development of EIEE in some patients. Determining whether other mutations in Munc18-1 act in a similar manner is an important future consideration.

EXPERIMENTAL PROCEDURES

Microscopy

PC12 cells or DKD-PC12 cells were transfected with Munc18-1 constructs using Lipofectamine LTX (Invitrogen) according to the manufacturer's instructions and expressed for 24–48 hr prior to replating onto poly-D-lysine-coated glass-bottomed MatTek dishes or glass coverslips. Cells were subsequently treated as described in the Results section and processed for either fluorescence microscopy (confocal microscopy or TIRF microscopy) or for correlative light and electron microscopy. Details are provided in the Supplemental Experimental Procedures.

Immunoprecipitation and Western Blotting

PC12 cells or DKD-PC12 cells were transfected with Munc18-1 constructs as described above. Cells were subsequently treated as described in the Results section and whole-cell lysates of Triton X-100 extracts analyzed by SDS-PAGE and western blotting. To analyze solubility, equivalent amounts of protein were solubilized in either 1% Triton X-100 (on ice; 60 min) or 1% SDS (20°C; 5 min). For immunoprecipitation, SDS-solubilized samples were subsequently diluted in 10% Triton X-100 to give a final concentration of 1% Triton X-100 and 0.1% SDS. GFP-tagged proteins were immunoprecipitated using GFP-Trap beads as described previously (Martin et al., 2013). Details are provided in the Supplemental Experimental Procedures.

NPY-hPLAP Release Assay

DKD-PC12 cells were cotransfected with NPY fused to the catalytic domain of human placental alkaline phosphatase (NPY-hPLAP) and the indicated Munc18-1 for 48 hr. Cells were washed and NPY-hPLAP release measured as described previously using the Phospha-Light chemiluminescent reporter gene assay system (Applied Biosystems), according to the manufacturer's instructions. The results are expressed as a percentage of total NPY-hPLAP. Details are provided in the Supplemental Experimental Procedures.

In Vitro Analyses

Isothermal titration calorimetry was performed using bacterially expressed recombinant protein as described previously (Deák et al., 2009; Christie et al., 2012). Full details are provided in the Supplemental Experimental Procedures. The *Leishmania tarentolae* extracts (LTE) were prepared as described previously (Kovtun et al., 2011). LTE-generated proteins were used to measure the interaction of Munc18-1WT and Munc18-1C180Y with Sx1a with a nanobead, ALPHAScreen assay. Single-molecule spectroscopy was performed as described previously (Sierecki et al., 2014; Gambin et al., 2014) following incubation of Munc18-1 or Munc18-1C180Y at different temperatures (30°C–40°C) for 15 or 30 min. Full details are provided in the Supplemental Experimental Procedures.

Statistical Analyses

Unless specified, statistical analysis was performed with an unpaired Student's t test assuming equal variance. Results shown are all mean ± SEM.

SUPPLEMENTAL INFORMATION

Supplemental Information includes Supplemental Experimental Procedures and three figures and can be found with this article online at http://dx.doi.org/10.1016/j.celrep.2014.08.059.

ACKNOWLEDGMENTS

This research was supported by a project grant from the National Health and Medical Research Council (NHMRC) of Australia (APP1044014 to F.A.M. and B.M.C.), an NHMRC Program Grant (APP1037320 to K.A.), and Australian Research Council (ARC) LIEF grants (LE130100078 and LE0882864 to F.A.M.). F.A.M. is a Senior Research Fellow of the NHMRC (APP569596). B.M.C. was supported by an ARC Future Fellowship (FT100100027) and currently holds an NHMRC Career Development Fellowship (APP1061574). Y.G. is supported by an ARC Future Fellowship (FT110100478). Electron microscopy was performed in the Australian Microscopy and Microanalysis Facility at the Centre for Microscopy and Microanalysis at the University of Queensland. The authors would like to thank R. Tweedale for critical reading of the manuscript.

Received: February 27, 2014
Revised: July 31, 2014
Accepted: August 23, 2014
Published: October 2, 2014

REFERENCES

Arunachalam, L., Han, L., Tassew, N.G., He, Y., Wang, L., Xie, L., Fujita, Y., Kwan, E., Davletov, B., Monnier, P.P., et al. (2008). Munc18-1 is critical for plasma membrane localization of syntaxin1 but not of SNAP-25 in PC12 cells. Mol. Biol. Cell *19*, 722–734.

Barcia, G., Chemaly, N., Gobin, S., Milh, M., Van Bogaert, P., Barnerias, C., Kaminska, A., Dulac, O., Desguerre, I., Cormier, V., et al. (2014). Early epileptic encephalopathies associated with STXBP1 mutations: Could we better delineate the phenotype? Eur. J. Med. Genet. *57*, 15–20.

Berke, S.J., and Paulson, H.L. (2003). Protein aggregation and the ubiquitin proteasome pathway: gaining the UPPer hand on neurodegeneration. Curr. Opin. Genet. Dev. *13*, 253–261.

Burkhardt, P., Hattendorf, D.A., Weis, W.I., and Fasshauer, D. (2008). Munc18a controls SNARE assembly through its interaction with the syntaxin N-peptide. EMBO J. *27*, 923–933.

Chen, Y.A., and Scheller, R.H. (2001). SNARE-mediated membrane fusion. Nat. Rev. Mol. Cell Biol. *2*, 98–106.

Christie, M.P., Whitten, A.E., King, G.J., Hu, S.H., Jarrott, R.J., Chen, K.E., Duff, A.P., Callow, P., Collins, B.M., James, D.E., and Martin, J.L. (2012). Low-resolution solution structures of Munc18:Syntaxin protein complexes indicate an open binding mode driven by the Syntaxin N-peptide. Proc. Natl. Acad. Sci. USA *109*, 9816–9821.

Deák, F., Xu, Y., Chang, W.P., Dulubova, I., Khvotchev, M., Liu, X., Südhof, T.C., and Rizo, J. (2009). Munc18-1 binding to the neuronal SNARE complex controls synaptic vesicle priming. J. Cell Biol. *184*, 751–764.

Deprez, L., Weckhuysen, S., Holmgren, P., Suls, A., Van Dyck, T., Goossens, D., Del-Favero, J., Jansen, A., Verhaert, K., Lagae, L., et al. (2010). Clinical spectrum of early-onset epileptic encephalopathies associated with STXBP1 mutations. Neurology *75*, 1159–1165.

Egri, C., and Ruben, P.C. (2012). A hot topic: temperature sensitive sodium channelopathies. Channels (Austin) *6*, 75–85.

Escayg, A., and Goldin, A.L. (2010). Sodium channel SCN1A and epilepsy: mutations and mechanisms. Epilepsia *51*, 1650–1658.

Gambin, Y., Ariotti, N., McMahon, K.A., Bastiani, M., Sierecki, E., Kovtun, O., Polinkovsky, M.E., Magenau, A., Jung, W., Okano, S., et al. (2014). Single-molecule analysis reveals self assembly and nanoscale segregation of two distinct cavin subcomplexes on caveolae. Elife *3*, e01434.

Han, L., Jiang, T., Han, G.A., Malintan, N.T., Xie, L., Wang, L., Tse, F.W., Gaisano, H.Y., Collins, B.M., Meunier, F.A., and Sugita, S. (2009). Rescue of Munc18-1 and -2 double knockdown reveals the essential functions of interaction between Munc18 and closed syntaxin in PC12 cells. Mol. Biol. Cell *20*, 4962–4975.

Han, G.A., Malintan, N.T., Collins, B.M., Meunier, F.A., and Sugita, S. (2010). Munc18-1 as a key regulator of neurosecretion. J. Neurochem. *115*, 1–10.

Han, G.A., Bin, N.R., Kang, S.Y., Han, L., and Sugita, S. (2013). Domain 3a of Munc18-1 plays a crucial role at the priming stage of exocytosis. J. Cell Sci. *126*, 2361–2371.

Jahn, R., and Fasshauer, D. (2012). Molecular machines governing exocytosis of synaptic vesicles. Nature *490*, 201–207.

Knaevelsrud, H., and Simonsen, A. (2010). Fighting disease by selective autophagy of aggregate-prone proteins. FEBS Lett. *584*, 2635–2645.

Komander, D., and Rape, M. (2012). The ubiquitin code. Annu. Rev. Biochem. *81*, 203–229.

Kovtun, O., Mureev, S., Jung, W., Kubala, M.H., Johnston, W., and Alexandrov, K. (2011). Leishmania cell-free protein expression system. Methods *55*, 58–64.

Malintan, N.T., Nguyen, T.H., Han, L., Latham, C.F., Osborne, S.L., Wen, P.J., Lim, S.J., Sugita, S., Collins, B.M., and Meunier, F.A. (2009). Abrogating Munc18-1-SNARE complex interaction has limited impact on exocytosis in PC12 cells. J. Biol. Chem. *284*, 21637–21646.

Martin, S., Tomatis, V.M., Papadopulos, A., Christie, M.P., Malintan, N.T., Gormal, R.S., Sugita, S., Martin, J.L., Collins, B.M., and Meunier, F.A. (2013). The Munc18-1 domain 3a loop is essential for neuroexocytosis but not for syntaxin-1A transport to the plasma membrane. J. Cell Sci. *126*, 2353–2360.

McEwen, J.M., and Kaplan, J.M. (2008). UNC-18 promotes both the anterograde trafficking and synaptic function of syntaxin. Mol. Biol. Cell *19*, 3836–3846.

Mignot, C., Moutard, M.L., Trouillard, O., Gourfinkel-An, I., Jacquette, A., Arveiler, B., Morice-Picard, F., Lacombe, D., Chiron, C., Ville, D., et al. (2011). STXBP1-related encephalopathy presenting as infantile spasms and generalized tremor in three patients. Epilepsia *52*, 1820–1827.

Otsuka, M., Oguni, H., Liang, J.S., Ikeda, H., Imai, K., Hirasawa, K., Imai, K., Tachikawa, E., Shimojima, K., Osawa, M., and Yamamoto, T. (2010). STXBP1 mutations cause not only Ohtahara syndrome but also West syndrome—result of Japanese cohort study. Epilepsia *51*, 2449–2452.

Papadopulos, A., Martin, S., Tomatis, V.M., Gormal, R.S., and Meunier, F.A. (2013). Secretagogue stimulation of neurosecretory cells elicits filopodial extensions uncovering new functional release sites. J. Neurosci. *33*, 19143–19153.

Price, J.L., and Morris, J.C. (1999). Tangles and plaques in nondemented aging and "preclinical" Alzheimer's disease. Ann. Neurol. *45*, 358–368.

Pridgeon, J.W., Webber, E.A., Sha, D., Li, L., and Chin, L.S. (2009). Proteomic analysis reveals Hrs ubiquitin-interacting motif-mediated ubiquitin signaling in multiple cellular processes. FEBS J. *276*, 118–131.

Saitsu, H., Kato, M., Mizuguchi, T., Hamada, K., Osaka, H., Tohyama, J., Uruno, K., Kumada, S., Nishiyama, K., Nishimura, A., et al. (2008). De novo mutations in the gene encoding STXBP1 (MUNC18-1) cause early infantile epileptic encephalopathy. Nat. Genet. *40*, 782–788.

Saitsu, H., Kato, M., Okada, I., Orii, K.E., Higuchi, T., Hoshino, H., Kubota, M., Arai, H., Tagawa, T., Kimura, S., et al. (2010). STXBP1 mutations in early infantile epileptic encephalopathy with suppression-burst pattern. Epilepsia *51*, 2397–2405.

Sierecki, E., Giles, N., Polinkovsky, M., Moustaqil, M., Alexandrov, K., and Gambin, Y. (2013). A cell-free approach to accelerate the study of protein-protein interactions in vitro. Interface Focus *3*, 20130018.

Sierecki, E., Stevers, L.M., Giles, N., Polinkovsky, M.E., Moustaqil, M., Mureev, S., Johnston, W.A., Dahmer-Heath, M., Skalamera, D., Gonda, T.J., et al. (2014). Rapid mapping of interactions between human SNX-BAR proteins measured in vitro by AlphaScreen and single-molecule spectroscopy. Mol. Cell. Proteomics *13*, 2233–2245.

Südhof, T.C., and Rizo, J. (2011). Synaptic vesicle exocytosis. Cold Spring Harb. Perspect. Biol. *3*, a00563.

Tavyev Asher, Y.J., and Scaglia, F. (2012). Molecular bases and clinical spectrum of early infantile epileptic encephalopathies. Eur. J. Med. Genet. *55*, 299–306.

Tomatis, V.M., Papadopulos, A., Malintan, N.T., Martin, S., Wallis, T., Gormal, R.S., Kendrick-Jones, J., Buss, F., and Meunier, F.A. (2013). Myosin VI small insert isoform maintains exocytosis by tethering secretory granules to the cortical actin. J. Cell Biol. *200*, 301–320.

Toonen, R.F., and Verhage, M. (2007). Munc18-1 in secretion: lonely Munc joins SNARE team and takes control. Trends Neurosci. *30*, 564–572.

Verhage, M., Maia, A.S., Plomp, J.J., Brussaard, A.B., Heeroma, J.H., Vermeer, H., Toonen, R.F., Hammer, R.E., van den Berg, T.K., Missler, M., et al. (2000). Synaptic assembly of the brain in the absence of neurotransmitter secretion. Science *287*, 864–869.

Voets, T., Toonen, R.F., Brian, E.C., de Wit, H., Moser, T., Rettig, J., Südhof, T.C., Neher, E., and Verhage, M. (2001). Munc18-1 promotes large dense-core vesicle docking. Neuron *31*, 581–591.

Weber, T., Zemelman, B.V., McNew, J.A., Westermann, B., Gmachl, M., Parlati, F., Söllner, T.H., and Rothman, J.E. (1998). SNAREpins: minimal machinery for membrane fusion. Cell *92*, 759–772.

Wickner, S., Maurizi, M.R., and Gottesman, S. (1999). Posttranslational quality control: folding, refolding, and degrading proteins. Science *286*, 1888–1893.

Wiese, C., and Zheng, Y. (2006). Microtubule nucleation: gamma-tubulin and beyond. J. Cell Sci. *119*, 4143–4153.

Yamamoto, A., and Simonsen, A. (2011). The elimination of accumulated and aggregated proteins: a role for aggrephagy in neurodegeneration. Neurobiol. Dis. *43*, 17–28.